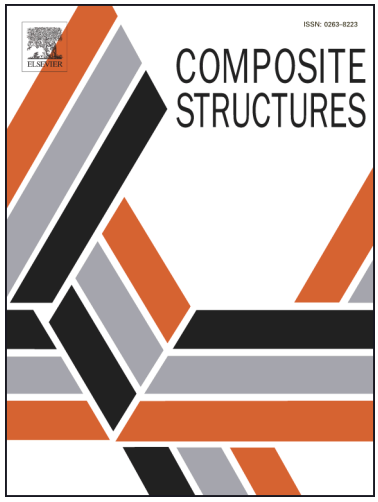

Determination of Mode I Dynamic Fracture Toughness of IM7-8552 Composites by Digital Image Correlation and Machine Learning

Rafael A. Cidade, Daniel S.V. Castro, Enrique M. Castrodeza, Peter Kuhn, Giuseppe Catalanotti, Jose Xavier, Pedro P. Camanho

PII: S0263-8223(18)32093-2
DOI: https://doi.org/10.1016/j.compstruct.2018.11.089
Reference: COST 10454

To appear in: *Composite Structures*

Received Date: 19 June 2018
Revised Date: 23 November 2018
Accepted Date: 30 November 2018

Please cite this article as: Cidade, R.A., Castro, D.S.V., Castrodeza, E.M., Kuhn, P., Catalanotti, G., Xavier, J., Camanho, P.P., Determination of Mode I Dynamic Fracture Toughness of IM7-8552 Composites by Digital Image Correlation and Machine Learning, *Composite Structures* (2018), doi: https://doi.org/10.1016/j.compstruct.2018.11.089

Determination of Mode I Dynamic Fracture Toughness of IM7-8552 Composites by Digital Image Correlation and Machine Learning

Rafael A. Cidade[1*], Daniel S.V. Castro[1], Enrique M. Castrodeza[1,2], Peter Kuhn[3], Giuseppe Catalanotti[4], Jose Xavier[5,6], Pedro P. Camanho[5,7]

[1] Department of Metallurgical and Materials Engineering, COPPE Federal University of Rio de Janeiro, P.O. Box 68505, 21941-972 Rio de Janeiro, Brazil

[2] Department of Mechanical Engineering, Politecnico di Milano, Via La Masa 1, 20156 Milano, Italy

[3] Department of Mechanical Engineering, Chair for Carbon Composites, Technical University of Munich, Boltzmannstraße 15, Garching, Germany

[4] Advanced Composites Research group (ACRG), School of Mechanical and Aerospace Engineering, Queen's University Belfast, Belfast BT9 5AH, UK

[5] Instituto de Ciência e Inovação em Engenharia Mecânica e Engenharia Industrial, Rua Dr. Roberto Frias, 400, 4200-465 Porto, Portugal

[6] UNIDEMI, New University of Lisbon, Faculty of Sciences and Technology, Department of Mechanical and Industrial Engineering, Campus de Caparica, Caparica, 2829-516, Portugal

[7] DEMec, Faculdade de Engenharia, Universidade do Porto, Rua Dr. Roberto Frias, s/n, 4200-465 Porto, Portugal

* Corresponding author: rafaelcidade@poli.ufrj.br

Abstract

An optical experimental procedure for evaluating the J-Integral from full-field displacement fields under dynamic loading is proposed in this work. The methodology is applied to measure the J-integral in the dynamic compressive loading of fiber-reinforced composites and to calculate the dynamic fracture toughness associated with the propagation of a kink-band. A modified J-Integral that considers inertia effects is calculated over the full-field measurements obtained by digital image correlation, for double edge-notched specimen of IM7-8552 laminates dynamically loaded in a split-

Hopkinson pressure bar (SHPB). A sensibility study is conducted to address the influence of the speckle parameters. The results show good agreement with experimental observations obtained by using a different data reduction method, suggesting the existence of a rising R-curve for the studied material under dynamic loading. Furthermore, it was noticed that the inertia effect can be negligible, indicating a state of dynamic equilibrium in which quasi-static approaches may comfortably be used.

Keywords: dynamic fracture toughness, digital image correlation (DIC), J-Integral, fiber-reinforced composite materials.

List of symbols

E_x, E_y, G_{xy}	longitudinal, transversal, and shear modulus
v_{xy}	in-plane Poisson coefficient
W	specimen half width
$a, a_0, \Delta a$	crack length, initial crack length, crack increment
$\dot{\epsilon}$	strain rate
SR	subset radius
NND	nearest neighbor distance
D	Feret diameter
J^d, j^d_{fit}	dynamic J-Integral, dynamic J-Integral fit
$u, \ddot{u}$	displacement field, acceleration field
x	in-plane direction
U	elastic energy
δ	Kronecker delta
σ	stress tensor

ρ	specific mass
q	weight function
A	area of a data point
dp	data point
c, h	domain width, domain height
Γ_i	inner contour region
G_C, G_{C0}, G_{C90}	laminate fracture toughness and fracture toughness of 0º and 90º plies
t, t_p	time frame, peak load time frame
$RI_{\%}$	variable relative importance
I_{ij}	input-hidden layer connection weights
Z_j	hidden layer-output connection weights
l, l_0	laminate thickness, thickness of 0º plies

Introduction

The compression failure in notched composites has been thoroughly studied with during the past decades [1] [2] [3] [4] [5]. Fiber-reinforced composites exhibit in compression a failure mechanism through the onset and propagation of kink bands [6, 2, 7, 8] that may be represented as cracks. Therefore, a fracture toughness is associated to the kink band failure mechanism. The fracture toughness is one of the key parameters used in strength prediction methods for composite materials. Its accurate determination is therefore essential and has given birth, in the past years, to the widespread development of different experimental techniques.

The experimental work performed has been mainly conducted under static loading conditions. The CT specimen ([9] [10] [11], among others) and the size effect method [12] have been used to measure the R-curve associated with the propagation of a kink-band. Despite the work performed so far only one paper [13] has been published on the

determination of dynamic compressive failure for fiber-reinforced composites. Considering that, in several real applications, composite structures need to withstand dynamic loading, it is necessary to further understand the dynamic behavior of this important class of materials.

Several works have studied the strain-rate dependence on fracture toughness of composite materials. Changes in the fracture toughness value have been explained by rate dependence on elastic properties as well as sensitivity of stress resistance limit [13] [14] [15] [16] [17]. This indicates a lack of consensus regarding the origin of the time dependent behavior, motivating effort toward this topic.

Many authors rely on quasi-static approaches on data reduction of their dynamic analysis, relying on the premise that dynamic stress equilibrium has been reached. Jiang and Vecchio [18] show in a review that the quasi-static theory is the preferred method to calculate fracture toughness under impact conditions, a conclusion reached by many other authors [19] [20] [21] [22] [23]. On the other hand, Nishioka [24] considers that the use of computer simulations is the only possible way to overcome difficulties in acquiring higher-order dynamic properties along a transient loading history.

Sun and Han [25] used the modified crack closure (MCC) integral to calculate mode I dynamic energy release rate of wedge loaded compact tension (WLCT) specimens using a finite elements formulation suggested by Jih and Sun [26]. The crack propagation is simulated by sequentially releasing the crack path nodes, based on experimental measurements of crack tip position, and the crack-closure integral calculated continuously trailing the crack-tip [27]. For Jih and Sun [26], an advantage of this method compared to the J-Integral is that it can easily separate the energy release rate for each fracture mode without knowing, *a priori*, the mixed-mode ratio. Navarro *et al.* [28] followed the work of Guo and Sun [29], which similarly to Sun and Hun [25], used the finite elements method with node releasing strategy to calculate mode I dynamic fracture toughness of carbon/epoxy and glass/epoxy composites. Differently from Jih and Sun [26], they used the energy balance (total strain-energy and total kinetic-energy) to calculate the energy release rate. Wu and Dzenis [30] also performed finite elements simulations on their dynamic delamination (Modes I and II) study. Instead of using a contour integral, like in the work presented by Sun and Han [25], they calculated stress intensity factors directly by the crack opening displacement, assuming an asymptotic displacement field near crack tip (Sih *et al.* [31]). The use of the crack opening

displacement instead of J-Integral was justified by the fact that the numerical differentiation step would reduce the accuracy of the analysis, since the stress field is calculated by the displacement derivative. In addition, it was pointed out that the dynamic path-independent integral would not avoid the singular stress field because it involves area integrals within the contour. Lee *et al.* [32] used the analytical expressions of the displacement field derived by Liu *et al.* [33] to calculate the dynamic stress intensity factor. Differently from Wu and Dzenis [30], where finite elements method was employed do calculate the crack opening displacement, they used 2D digital image correlation (DIC) and high-speed photography to obtain the full-field displacements and further calculate the dynamic stress intensity factors. An analogous approach was used by Joudon *et al.* [34] for the measurement of the dynamic mode I fracture toughness of toughened epoxy resins. The authors used a strain gage method instead of DIC, following the work of Khanna and Shukla [35], which assumes an asymptotic strain field near the tip of a moving crack with constant velocity. Additionally, the authors mentioned that the local analysis of asymptotic fields are preferred on determining fracture mechanics parameters during fast propagating cracks on brittle polymers. Kunh *et al.* [13] studied the dynamic compression toughness for carbon/epoxy under a strain rate of $100s^{-1}$. The approach presented uses the relations between the size effect law, proposed by Bažant *et al.* [36], the energy release rate and R-curve, under a quasi-static assumption, reporting a significant increase in the fracture toughness. In agreement with Wosu *et al.* [21], they reported a negligible influence of the kinetic energy in total process energy, justifying the use of the quasi-static approach.

The use of J-Integral over full-field measurements has also been proposed. Jiang *et al.* [37] calculated the value of the J-Integral, under quasi-static regime, for composite materials used in dental restorations over full-field measurements obtained by DIC and reported no considerable dependence on size and location of the integration path, concluding that the J-Integral calculation aside the DIC, is a reliable technique for calculating the material fracture toughness. Similar results were found in other studies, confirming the reliability of the use of J-Integral over full-field measurements [38] [39] [9]. In addition, the use of the area domain J-Integral has been reported by some authors as an advantageous alternative to the traditional contour J-Integral, regarding the integration domain dependency and the error reduction [40] [41].

To achieve a reliable DIC, the subset size must be trade-off between the capacity of distinguishing it from different subsets and avoiding mask heterogeneities in full-field measurements by using a large window. Additionally, small subsets would lead to an increase of local correlation coefficient minimums, decreasing the technique efficiency [42]. Studies have been done towards finding the optimal subset values, considering the image and the speckle pattern properties. A practical suggestion is the use of a subset size that circumscribes at least three speckle particles. Leading to the development of geometric models for determining the optimal subset size [43] [44] [45] [46] [47] [48] [49].

However, all the studies performed using J-Integral and DIC were done in quasi-static conditions and didn't evaluated the J results sensitivity in relation to the parameters used in DIC and in the formulation of J-Integral, although there are some works that evaluate the influence of DIC parameters in strain error. Thus, this work aims to analyse, by using artificial neural networks, the influence of the parameters used for J calculation. In addition, it is discussed the application of an inertial term in the J integral and the possibility of the construction of a dynamic R curve based on fracture toughness results.

This work is complementary to thse published by Kuhn *et al.* [13]. Therefore, it is discussed the determination of the dynamic fracture toughness of the tested material by two different methodologies: the analytical model presented by Catalanotti *et al.* [9] [12], and the DIC analysis, proposed in this paper.

Materials and Methods

Material and tests specimens.

Flat panels with a 4 mm thickness and a layup of $[90/0]_{8S}$ were manufactured using HexPly IM7-8552 carbon-epoxy prepreg system. The panel was cured by hot-pressing following the curing cycle suggested by the manufacturer [50]. Table 1 shows the elastic properties of the laminate measured under high strain ($\dot{\epsilon} = 100s^{-1}$) [13].

High strain rate fracture tests were carried out on double-edge notched in compression (DENC) specimens machined from the panel by a 1 mm drill bit. The specimens have all the same shape but different sizes, or in other word, the width and the length of the

specimen are proportional to a characteristic size, W, as indicated in Figure 1. Table 2 shows the dimensions used in this experimental campaign.

For the assessment of full-field displacements by the DIC technique the specimens were covered by a random black and white speckle pattern.

Experimental setup and high strain rate tests

The high strain rate tests were performed in a split-Hopkinson pressure bar (SHPB). Different bar diameters and pulse shapers were used to achieve the same strain rate for all specimens ($\dot{\epsilon} = 100 s^{-1}$). A high-performance PHOTRON AS-Z camera was used to capture the speckle pattern variation along time. The acquisition frequency and the resolution were 300,000 fps 256 x 128 pixels^2, respectively. Further details of the experimental setup can be found in [13].

Full field measurements (DIC)

Subset determination model

Aiming for a good analysis of deformations by the DIC method, the ideal size of the subset radius to be used must be determined. It will determine the size of the window for which the occurred displacement identification is made according to the change of location of sets of points at different gray scale values. In order to respect the requirements of having at least 3 speckles by subset [48] and to ensure the best possible resolution, a geometric model, in which the speckles are considered perfectly circular and their centers are located at the vertices of an equilateral triangle, is proposed. This is the most homogeneous arrangement for three points around the same reference point. Therefore, the model considers the distance between the centers of the circles as the nearest neighbor distance (NND) and that the diameter of the circles as the speckles Feret diameter (D) [51], as shown in Figure 2.

The considered value for the speckle size is that which covers 95% of the particles Feret diameter distribution, ensuring a wide range of particles size within the subset. Analogously, the free path between particles considered is that in respect of 95% of the nearest neighbor distance distribution (NND). By using Euclidian geometry, the subset radius value (SR), that is equivalent to de distance between de triangle center and the circumference that circumscribes the three small circles, is calculated by Equation 1.

$$SR = D_{95\%} + NND_{95\%}\frac{\sqrt{3}}{3} \quad \text{Equation 1}$$

To obtain the speckles Feret diameter and the free path distributions, image processing techniques were performed in steps, illustrated in Figure 3, using the open source software ImageJ® [52], following the sequence below:

a) Histogram equalization: To enhance the contrast by stretching out the intensity distribution to the whole range of intensity spectrum.

b) Classification: The image is made binary by using the Bernsen adaptive threshold filter [53], with a 15 × 15 px² window. The resulting black regions refer to the particles while white regions refer to the background.

c) Watershed: to avoid overestimating the particles size by separating touching objects.

d) Area filter and despeckle: To remove particles smaller than 4 px² and smooth sharp regions of particles.

Full field measurements

The full field measurements (displacements and strains) were calculated by the DIC technique, using the open-source DIC software Ncorr [42]. The subset size for each specimen was determined by the procedure descripted previously. Green-Lagrange strains are calculated by Ncorr, using the strain-displacement relation with small deformation formulation (Equation 2). Ncorr uses piecewise least-squares fitting over a region of the displacement field data points, the strain window, to calculate the displacements gradient (∇u). The size of the strain window will be discussed further.

$$\epsilon = \frac{1}{2}\left(\frac{\Delta u_i}{\Delta x_j} + \frac{\Delta u_j}{\Delta x_i}\right) \quad \text{Equation 2}$$

Dynamic J-Integral calculation

Formulation

In this study an implementation of the J-Integral proposed by Atluri [54] and used in Kuna [55] is proposed. It considers the inertia effect and neglects the kinetic energy, for the case of dynamically loaded stationary cracks.

The J-Integral is calculated for each notch, and the higher value is taken. The discrete implementation of the J-Integral is the sum of the contribution of each individual data point within the domain boundaries and A represents the area of a data point, in mm².

$$J^d = \sum_{dp}\left\{\left[\left(U\delta_{i2} - \sigma_{i2}\frac{\Delta u_i}{\Delta x_2}\right)\frac{\Delta q}{\Delta x_j} + \rho\frac{\Delta u_i}{\Delta x_j}\ddot{u}_i q\right]A\right\}_{dp} \qquad \text{Equation 3}$$

The domain transformation, from contour to area, requires the use of a weight function q, that must follow two requirements:

1. Must vary smoothly from 0 (at the outer contour) to 1 (at the inner contour).
2. Must value 1 within the inner contour (in the present case the inner contour $\Gamma_i \to 0$).

In the discrete implementation, the operator $\Delta/\Delta x_j$ represents the gradient vector, where Δx is the length represented by a data point edge. The J-Integral was calculated for every time step (i.e. image frames), so that a behavior over time can be obtained. The chosen function is a biquadratic equation, shown in Equation 4, which satisfies the mentioned conditions.

$$q(x,y) = \left(\frac{c^2-x^2}{c^2}\right)\left(\frac{h^2-y^2}{h^2}\right) \qquad \text{Equation 4}$$

In the proposed methodology the weight function is also responsible for the domain boundaries determination. Since it only has values within the outer contour and the J-Integral terms multiply q and ∇q, the J-Integral area domain can be set by the parameters c and h (i.e. the width and the height of function domain). Figure 5 shows the biquadratic equation for a domain with 170 × 65 data points.

Fracture toughness definition

In this study, the initiation fracture toughness is defined as the point of instability, assumed as the point of the peak load during the test [13] [12]. Considering the linear-elastic behavior of the material, G_C is defined as:

$$G_C = J^d\big|_{t=t_p} \qquad \text{Equation 5}$$

The fracture toughness calculation consisted in a polynomial fit of the J-Integral values over time for all specimens of each type. A window of 23 consecutive frames, which comprises all the experimental fracture process, was used. The 21st frame matches the peak load time ($t = t_p$), so all specimens of each type could be synchronized by the peak

load frame and plot over the same time domain, as can be seen on Figure 6. Further, a third order polynomial was used to fit the J-Integral over time and the value of $J_{fit}^{d}\big|_{t=t_p}$ is assumed to be the initiation fracture toughness.

Parameters sensitivity analysis

The influence of three parameters were assessed in this study: the strain window, the domain width (*c*), and the domain height (*h*), as shown in Figure 4.

Full factorial design

A full factorial design was generated to evaluate de influence of the parameters on J-Integral value. Three parameters were chosen for assessing the robustness of the method: the strain window, the domain height, and the domain width.

- The strain window relates to the sensitivity of the J-Integral regarding the smoothness of the strain field.
- The domain size variation verifies whether the area domain J-Integral is dependent to the integration domain, analogous to the path independence of the classic J-Integral.

Five levels, shown in Table 3, were heuristically chosen for each parameter.

Analysis of Parameters Relative Importance ($RI_{\%}$)

Lilliefors' tests [56] have shown that the J-Integral residuals do not fit in a normal distribution regarding the variation of the parameters. So, it would not be appropriate to evaluate the effect of the variables using the ANOVA method. The connection weights (CWM) method was used to estimate RI for each variable based on the weights of a trained artificial neural network (ANN) [57]. The relative importance of a given input variable can be defined by Equation 6, for the case of a single hidden layer.

$$RI_i = \sum_{h=1}^{n} I_{ij} Z_j \qquad \text{Equation 6}$$

where, n is the total number of hidden nodes, I_{ij} is the weight of the connections between input nodes and hidden nodes, and Z_j is the weight of the connection between hidden nodes and the output node. In this study, a multilayer perceptron (MLP) ANN with four hidden neurons within a single hidden layer (Figure 7) was heuristically chosen to evaluate the $RI_{\%}$ of input variables.

Results and discussion

Subset Size

Table 4 shows the results for the subset size for each specimen type, and its respective input parameters (Feret diameter and NND).

The scale factor increases with the decrease of the specimen size (i.e. the zoom in smaller specimens has great magnitude compared to larger specimens), therefore all specimens present approximately the same size in pixels. Considering the speckle particles distribution to be the same for all specimens (the same application method was used), Larger specimens are expected to present smaller speckle particles, in pixels. Consequently, decreasing subset size.

Dynamic Fracture Toughness

The above defined initiation fracture toughness criterion was applied to all specimens. Figure 8 shows the J-Integral over time and the polynomial fit for type II. The initial point, or *0s*, refers to the 20^{th} frame before the peak load frame. It is a representative curve that follows the other types.

Computing the fracture toughness for all specimens, it was possible to evaluate the sensitivity of its value regarding the variation of the method parameters. The connection weights method [57] indicates that the greatest relative influence comes from the domain height (i.e. along crack direction), as shown in Figure 9.

Table 5 shows the fracture toughness and its standard deviation for three scenarios:

- 3 parameters variation: the full factorial design.
- 2 parameters variation: strain window fixed at a value of 9 data points, and the domain parameters varying from 50% to 90% of the specimen size in the respective direction.
- 1 parameter variation: strain window fixed at a value of 9 data points, the domain width fixed at 90% of specimen width, varying the domain height from 50% to 90% of the specimen half height (W).

The results show an increasing trend of the dynamic fracture toughness in respect of specimen size. Considering that different sizes relate to different notch sizes (a_0), it is

plausible the existence of a rising R-Curve for the IM7-8552 under dynamic loads, as expected. Since the R-Curve of a given material is invariant, in the present case in which a_0/W is constant greater test specimens are expected to achieve instability at greater G_C values. This result agrees to the results obtained by Kuhn *et al.* [13], which calculated a R-curve of the same material based on the method proposed by Catalanotti *et al.* [12]. This method relies on the relation between the energy release rate and the size-effect law established by Bažant *et al.* [36].

The method used by Kuhn *et al.* [13] to establish the relation between W and Δa was applied to the results obtained in the present paper. Figure 10 shows the average initiation fracture toughness of the full factorial design (Figure 8) and the R-curve obtained by Kuhn *et al* [13].

The R-Curve calculated by Kuhn *et al.* [13], for longitudinal plies, was compared to the fracture toughness results calculated in the present work (Equations 5 and 7), neglecting the transversal plies contribution ($G_{C0} \gg G_{C90}$), following Pinho *et al.* [10].

$$G_{C0} = \frac{l}{l_0} G_C. \qquad \text{Equation 7}$$

An important remark is that, differently from Kuhn *et al.* that obtained the R-Curve based on the size effect law applied on the specimens' ultimate stress, the present work calculates the G_C values based on full-field measurements, without using load information (except for the peak load time frame, t_p). The close agreement of the results indicates that the proposed methodology could be a reliable alternative for fracture toughness determination of composite laminates subjected to dynamic loads. Table 6 shows a comparison to values found in previous works for the same tested material. The same consideration of longitudinal fracture toughness applies (Equation 7).

Regarding the domain dependence on fracture toughness value (Table 5) the greatest variation coefficient is 7.8%, for the type II in full factorial scenario. It shows that the dynamic fracture toughness does not depend significantly on the chosen area domain.

Inertia Effect

The fracture toughness calculation applied in this work (Equation 3), allows the assessment of the inertial term $\left(\rho \frac{\Delta u_i}{\Delta x_j} \ddot{u}_i q\right)$ contribution on total J-Integral value. It was found that the inertia contribution is negligible for all analyzed specimens,

approximately 0.01%, 0.10%, and 0.35% of the total fracture toughness, for types I, II and, III respectively, suggesting the achievement of the dynamic equilibrium, agreeing with Kuhn *et al.* [13] on the reliability of the quasi-static methodology for the dynamic analysis. Moreover, a rising trend can be observed indicating the larger the specimens, the higher the inertial term is, even though it is negligible in the present study. This trend could be related to the time to achieve the dynamic equilibrium, that is longer for larger specimens [58].

Conclusions

The main conclusions outlined in this study can be summarized as follows:

- The modified J-Integral calculated in this study makes possible the evaluation whether the dynamic equilibrium have been achieved, by the analysis of the inertial term against the total energy release rate value.
- The proposed methodology for measuring the J-integral from full-field displacement provided by DIC is shown to be stable with regard to setting parameters. The results show a small variation coefficient regarding the DIC and the integration domain parameters.
- Machine learning was useful on assessing the relative influence of the input variables. The use of the weights of a trained artificial neural network was an alternative in the present case, where statistical distributions could not be applied.
- The results show a rising trend on the fracture toughness in respect of the increase of the specimen size, and consequently the increase of a_0, suggesting the existence of a rising R-curve.
- Present results and those from Kuhn *et al.* [13] are in close agreement, even though they come from two different methodologies, with non-related input variables.

Acknowledgements

To both the Brazilian National Council for Scientific and Technological Development (CNPq) for the split-site doctoral program scholarship at Faculdade de Engenharia da Universidade do Porto (under grant no. 206575/2014-9), and to the Brazilian National Council for the Improvement of Higher Education (CAPES) for the doctoral scholarship of Rafael Cidade. P. P. Camanho would like to acknowledge the funding of Project NORTE-01-0145-FEDER-000022 - SciTech - Science and Technology for Competitive and Sustainable Industries), co-financed by Programa Operacional Regional do Norte NORTE2020, through Fundo Europeu de Desenvolvimento Regional (FEDER).

References

[1] T. J. Vogler and S. Kyriakides, "On the axial propagation of kink bands in fiber composites : Part I experiments," *International Journal of Solids and Structures*, vol. 36, no. 47, pp. 557-574, 1999.

[2] B.Budiansky and N.A.Fleck, "Compressive failure of fibre composites," *Journal of the Mechanics and Physics of Solids*, vol. 41, no. 1, pp. 183-211, 1993.

[3] T. J. Vogler and S. Kyriakides, "On the initiation and growth of kink bands in fiber composites: Part I. experiments," *International Journal of Solids and Structures*, vol. 38, no. 15, pp. 2639-2651, 2001.

[4] S. Y. Hsu, T. J. Vogler and S. Kyriakides, "Compressive strength predictions for fiber composites," *ASME J. Appl. Mech.*, vol. 65, pp. 7-16, 1998.

[5] S. K. Kyriakides, R. Arseculeratne, E. J. Perry and K. M. Liechti, "On the compressive failure of fiber reinforced composites," *Intl J. Solids and Structures*, vol. 32, pp. 689-738, 1995.

[6] J. Patel, "Mechanisms for Kink Band Evolution in Polymer Matrix Composites: A Digital Image Correlation and Finite Element Study," 2016.

[7] A. Argon, "Fracture of Composites," *Treatise on Materials Science & Technology*, vol. 1, pp. 79-114, 1972.

[8] P. Moran and C. Shih, "Kink band propagation and broadening in ductile matrix fiber composites: Experiments and analysis," *International Journal of Solids and Structures*, vol. 35, no. 15, pp. 1709-1722, 1998.

[9] G. Catalanotti, A. T. Marques, C. G. Dávila, J. Xavier and P. P. Camanho, "Measurement of resistance curves in the longitudinal failure of composites using digital image correlation," *Composites Science and Tachnology*, vol. 70, no. 13, pp. 1986-1993, 2010.

[10] S. T. Pinho, P. Robinson and L. Iannucci, "Fracture toughness of the tensile and compressive fibre failure modes in laminated composites," *Composites Science and Technology*, vol. 66, pp. 2069-2079, 2006.

[11] M. S. Prasad, C. Venkatesha and T. Jayaraju, "Experimental Methods of Determining Fracture Toughness of Fiber Reinforced Polymer Composites under Various Loading Conditions," *Journal of Minerals & Materials Characterization & Engineering*, vol. 10, no. 13, pp. 1263-1275, 2011.

[12] G. Catalanotti, J. Xavier and P. P. Camanho, "Measurement of the compressive crack resistance curve of composites using the size effect law," *Composites Part A: Applied Science and Manufacturing*, vol. 56, pp. 300-307, 2014.

[13] P. Kuhn, H. Koerber, G. Catalanotti, J. Xavier and P. P. Camanho, "Fracture toughness and crack resistance curves for fiber compressive failure mode in polymer composites under high rate loading," *Composite Structures*, vol. 182, no. 15, pp. 164-175, 2017.

[14] H. M. Hsiao and I. Daniel, "Strain rate behavior of composite materials," *Composites Part B-Engineering*, vol. 29, no. 5, pp. 521-533, 1998.

[15] Q. Bing and C. T. Sun, "Modeling and testing strain rate-dependent compres- sive strength of carbon/epoxy composites," *Composites Science and Technology*, vol. 65, no. 15-16, pp. 2481-2491, 2005.

[16] H. Koerber and P. P. Camanho, "High strain rate characterisation of unidirectional carbon–epoxy IM7-8552," *Composites: Part A*, vol. 42, no. 11, pp. 462-470, 2011.

[17] T. Yokoyama and T. Nakai, "Impact compressive failure of a unidirectional carbon/epoxy laminated composite in three principal material directions," in *Proceedings of DYMAT 2009 conference*, Brussels, 2009.

[18] F. Jiang and K. S. Vecchio, "Hopkinson Bar Loaded Fracture Experimental Technique : A Critical Review of Dynamic," *Applied Mechanics Reviews*, vol. 62, no. 6, 2009.

[19] R. Fracasso, M. Rink, A. Pavan and R. Frassine, "The effects of strain-rate and temperature on the interlaminar fracture toughness of interleaved PEEK/CF composites," *Composites Science and Technology*, vol. 61, no. 1, pp. 57-63, 1 2001.

[20] S. N. Wosu, D. Hui and P. K. Dutta, "Dynamic mode II delamination fracture of unidirectional graphite/epoxy composites," *Composites Part B: Engineering,* vol. 34, no. 3, pp. 303-316, 4 2003.

[21] S. N. Wosu, D. Hui and P. K. Dutta, "Dynamic mixed-mode I/II delamination fracture and energy release rate of unidirectional graphite/epoxy composites," *Engeneering Fracture Mechanics,* vol. 72, no. 10, p. 1531–1558, August 2005.

[22] M. Colin de Verdiere, A. A. Skordos, A. C. Walton and M. May, "Influence of loading rate on the delamination response of untufted and tufted carbon epoxy non-crimp fabric composites/Mode II," *Engineering Fracture Mechanics,* vol. 96, pp. 1-10, 2012.

[23] H. Zabala, L. Aretxabaleta, G. Castillo and J. Aurrekoetxea, "Loading rate dependency on mode I interlaminar fracture toughness of unidirectional and woven carbon fibre epoxy composites," *Composite Structures,* vol. 121, pp. 75-82, 2015.

[24] T. Nishioka, "Computational dynamic fracture mechanics," *International Journal of Fracture,* vol. 86, no. 1-2, pp. 127-159, 1997.

[25] C. T. Sun and C. Han, "A method for testing interlaminar dynamic fracture toughness of polymeric composites," *Composites Part B: Engineering,* vol. 35, no. 6-8, pp. 647-655, 9 2004.

[26] C. J. Jih and C. T. Sun, "Evaluation of a finite element based crack-closure method for calculating static and dynamic strain energy release rates," *Engineering Fracture Mechanics,* vol. 37, no. 2, pp. 313-322, 1990.

[27] J. F. Malluck and W. W. King, "Fast Fracture Simulated by Conventional Finite Elements: A Comparison of Two Energy-Release Algorithms," *ASTM STP711,* pp. 38-53, 1980.

[28] P. Navarro, J. Aubry, F. Pascal, S. Marguet, J. F. Ferrero and O. Dorival, "Influence of the stacking sequence and crack velocity on fracture toughness of woven composite laminates in mode I," *Engineering Fracture Mechanics,* vol. 131, pp. 340-348, 2014.

[29] C. Guo and C. T. Sun, "Dynamic Mode-I crack-propagation in a carbon/epoxy composite," *Composites Science and Technology,* vol. 58, no. 9, pp. 1405-1410, 1998.

[30] X. F. Wu and Y. a. Dzenis, "Determination of dynamic delamination toughness of a graphite-fiber/epoxy composite using hopkinson pressure bar," *Polymer Composites,* vol. 26, no. 2, pp. 165-180, 2005.

[31] G. C. Sih, P. C. Paris and G. R. Irwin, "On cracks in rectilinearly anisotropic bodies," *International Journal of Fracture Mechanics,* vol. 1, no. 3, pp. 189-203, 1965.

[32] D. Lee, H. Tippur and P. Bogert, "Quasi-static and dynamic fracture of graphite/epoxy composites: An optical study of loading-rate effects," *Composites Part B: Engineering,* vol. 41, no. 6, pp. 462-474, 2010.

[33] C. Liu, A. J. Rosakis and M. G. Stout, "Dynamic Fracture Toughness of a Unidirectional Graphite / Epoxy Composite," in *Proceedings of the Symposium on Dynamic Effects in Composite Structures,* New York, 2001.

[34] V. Joudon, G. Portemont, F. Lauro and B. Bennani, "Experimental procedure to characterize the mode I dynamic fracture toughness of advanced epoxy resins," *Engineering Fracture Mechanics,* vol. 126, pp. 166-177, 2014.

[35] S. K. Khanna and A. Shukla, "On the use of strain gages in dynamic fracture mechanics," *Engineering Fracture Mechanics,* vol. 51, no. 6, pp. 933-948, 1995.

[36] Z. Bazant, J. H. Kim, I. M. Daniel, E. Becq-Giraudon and G. Zi, "Size effect on compression strength of fiber composites failing by kink band propagation," *International Journal of Fracture,* vol. 95, pp. 103-141, 1999.

[37] Y. Jiang, A. Akkus, R. Roperto, O. Akkus, B. Li, L. Lang and S. Teich, "Measurement of J-integral in CAD/CAM dental ceramics and composite resin by digital image correlation," *Journal of the mechanical behavior of biomedical materials,* vol. 62, p. 240—246, 9 2016.

[38] G. L. G. Gonzáles, J. A. O. González, J. T. P. Castro and J. L. F. Freire, "A J-integral approach using digital image correlation for evaluating stress intensity factors in fatigue cracks with closure effects," *Theoretical and Applied Fracture Mechanics,* vol. 90, pp. 14-21, 2017.

[39] K. Allaer, I. D. Baere, W. V. Paepegem and J. Degrieck, "Direct fracture toughness determination of a ductile epoxy polymer from digital image correlation measurements on a single edge notched bending sample," *Polymer Testing,* vol. 42, pp. 199-207, 2015.

[40] F. Z. Li, C. F. Shih and A. Needleman, "A comparison of methods for calculating energy release rates," *Engineering Fracture Mechanics,* vol. 21, no. 2, pp. 405-421, 1985.

[41] T. H. Becker, M. Mostafavi, R. B. Tait and T. J. Marrow, "An approach to calculate the J-integral by digital image correlation displacement field measurement," *Fatigue \& Fracture of Engineering Materials \& Structures,* vol.

35, no. 10, pp. 971-984, 2012.

[42] Y. Huang, "Development of digital image correlation method for displacement and shape measurement," Singapore, 2004.

[43] J. Zhang, G. C. Jin, S. P. Ma and L. B. Meng, "Application of an improved subpixel registration algorithm on digital speckle correlation measurement," *Optics and Laser Tech*, vol. 35, no. 7, pp. 533-542, 2003.

[44] D. Lecompte, A. Smitsb, S. Bossuytb, H. Solb, J. Vontommea, D. V. Hemelrijck and A. M. Habraken, "Quality assessment of speckle patterns for digital image correlation," *Optics and Lasers in Engineering*, vol. 44, no. 11, pp. 1132-1145, 2006.

[45] Y. P. H. Sun, Y. F. Sun and H. L. Pang, "Study of optimal subset size in digital image correlation of speckle pattern images," *Optics and Lasers in Eng*, vol. 45, no. 9, pp. 967-974, 2007.

[46] H. Ã. Haddadi and S. Belhabib, "Use of rigid-body motion for the investigation and estimation of the measurement errors related to digital image correlation technique," *Optics and Lasers in Engineering*, vol. 46, no. 2, pp. 185-196, 2008.

[47] G. Lionello and L. Cristofolini, "A practical approach to optimizing the preparation of speckle patterns for digital-image correlation," *Measurement Science and Technology*, vol. 25, 2014.

[48] K. A. Kasvayee and L. Elmquist, "Development of a Pattern Making Method for Strain Measurement on Microstructural Level in Ferritic Cast Iron," *Processing and Fabrication of Advanced Materials*, 2014.

[49] M. A. Sutton, J. J. Orteu and H. W. Schreier, Image Correlation for Shape and Deformation Measurements: Basic Concepts, Theory and Applications, New York, NY: Springer, 2009.

[50] "Material Data Sheet. HexPly 8852 Product Data," 2013.

[51] H. G. Merkus, Particle Size Measurements: Fundamentals, Practice, Quality, Springer, 1999.

[52] C. A. Schneider, W. S. Rasband and K. W. Eliceiri, "NIH Image to ImageJ: 25 years of image analysis," *Nature methods*, vol. 9, no. 7, pp. 671-675, 2012.

[53] J. Bernsen, "Dynamic thresholding of grey-level images," in *Proc. 8th International Conference on Pattern* , Paris, 1986.

[54] S. N. Atluri, "Path-indepent integrals in finite elasticity and inelasticity, with body forces ,inertia and arbitrary crack-face conditions," *Engineering Fracture Mechanics*, vol. 16, no. 3, pp. 341-364, 1982.

[55] M. Kuna, Finite Elements in Fracture Mechanics, Springer Netherlands, 2013.

[56] H. W. Lilliefors, "On the Kolmogorov-Smirnov Test for Normality with Mean and Variance Unknown," *Journal of the American Statistical Association*, vol. 62, no. 318, pp. 399-402, 1967.

[57] J. D. Olden and D. A. Jackson, "Illuminating the “black box”: a randomization approach for understanding variable contributions in artificial neural networks," *Ecological Modelling*, vol. 154, no. 1-2, pp. 135-150, 2002.

[58] N. S. Al-Maliky, "Dimension Effect on Dynamic Stress Equilibrium in SHPB Tests," *International Journal of Materials Physics*, vol. 5, no. 1, pp. 15-26, 2014.

Table 1: Laminate elastic properties for high strain rate.

$E_x = E_y$ (GPa)	G_{xy} (GPa)	v_{xy}
67.126	6.345	0.04

Table 2: Nominal dimensions of the specimens (all values in mm).

Specimen type	I	II	III
a_0	2.50	3.75	6.75
W	5.00	7.50	12.50

Table 3: Parameters and parameter levels of the full factorial design.

Parameter	Level 1	Level 2	Level 3	Level 4	Level 5

Strain window (data points)	10	14	18	22	26
Domain height	50%	60%	70%	80%	90%
Domain width	50%	60%	70%	80%	90%

Table 4: Results for the subset size for each specimen type (all values in pixels).

Specimen type	D	NND	SR
I	17 ± 1	11 ± 1	15 ± 0
II	12 ± 2	11 ± 1	13 ± 4
III	10 ± 1	10 ± 1	11 ± 2

Table 5: Mean fracture toughness results and standard deviation (in kJ/m²) regarding the variation of the factorial design parameters.

Specimen type	3 parameters	2 parameters	1 parameter
I	61.8 ± 2.4	61.7 ± 1.3	59.4 ± 1.2
II	67.6 ± 5.3	68.6 ± 3.4	66.4 ± 3.9
III	91.3 ± 4.0	91.6 ± 2.7	88.4 ± 3.0

Table 6: Comparison of the determined fracture toughness value for IM7-8552 longitudinal plies with previous works[1].

Author	Regime	G_C (kJ/m²)
Present study (DIC)	$\dot{\epsilon} = 100s^{-1}$	$\approx 120 - 180$

[1] The values related to Kuhn *et al.* [13] and Catalanotti *et al.* [12] refer to the steady-state fracture toughness value.

Kuhn *et al.* [13]	$\dot{\epsilon} = 100s^{-1}$	≈ 165
Kuhn *et al.* [13]	Quasi-static	≈ 101
Catalanotti *et al.* [12]	Quasi-static	≈ 61

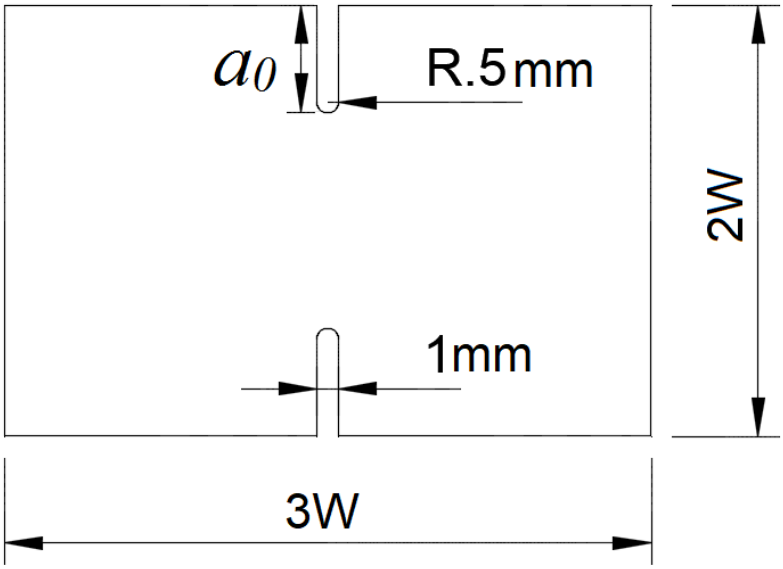

Figure 1 - Specimen geometry.

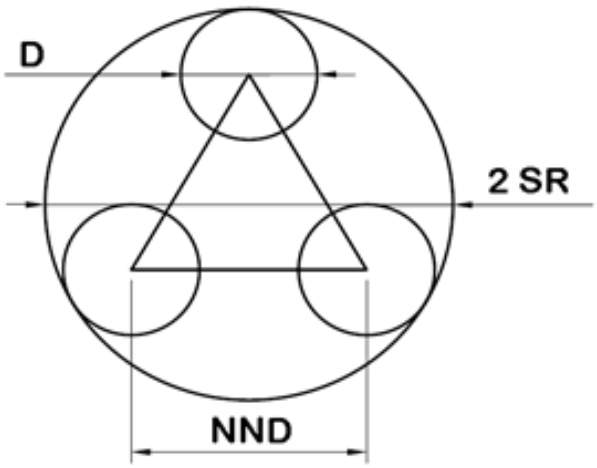

Figure 2 – Geometric model for subset radius.

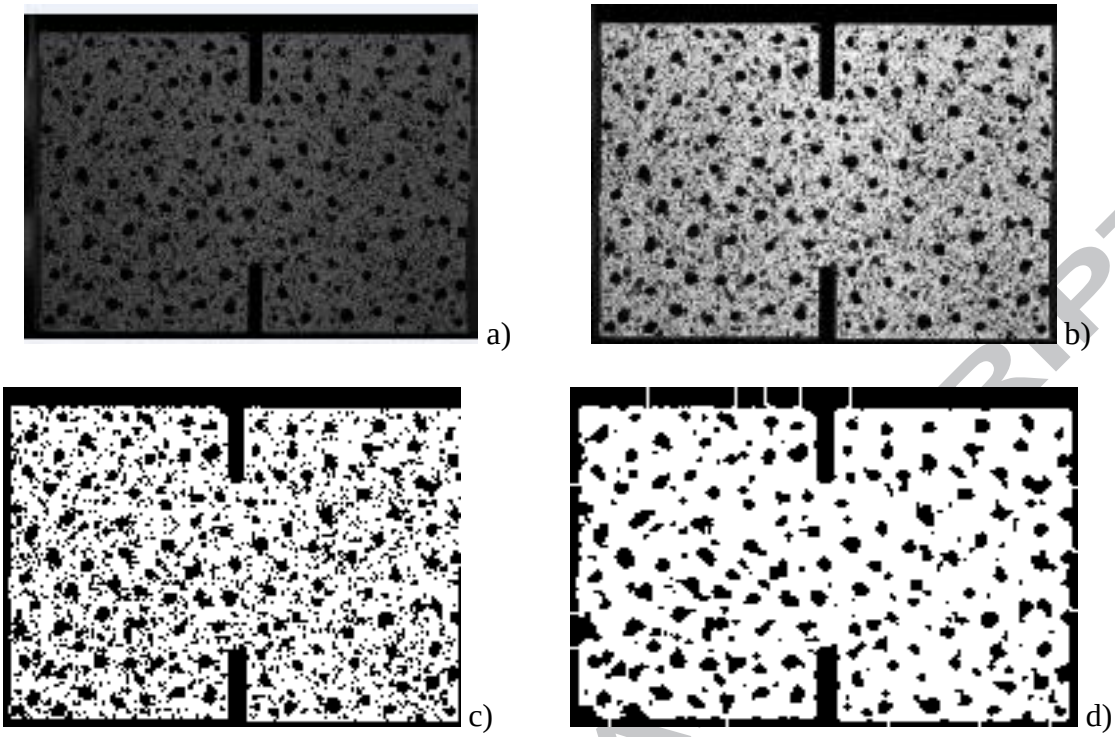

Figure 3 – a) Original image; b) Equalized image; c) Binary image; and d) Final image after watershed and size filtering.

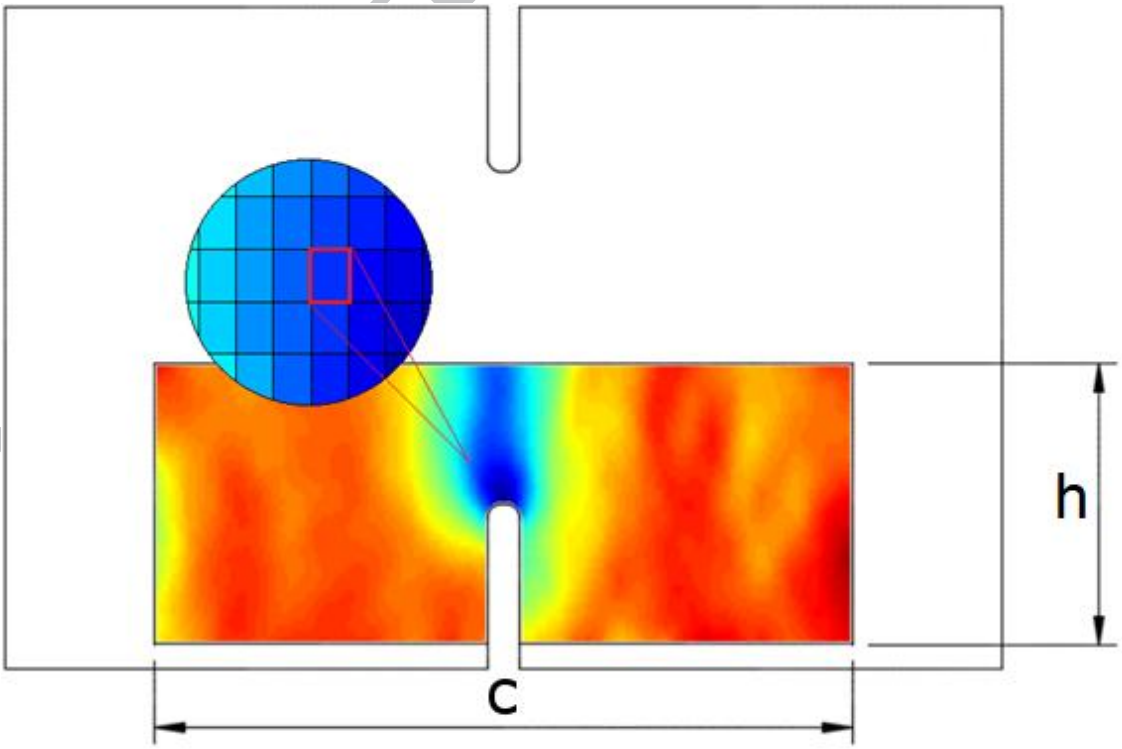

Figure 4 - An illustration of a stress field within a domain of size $c \times h$ including the notch, showing a single data point, marked in red.

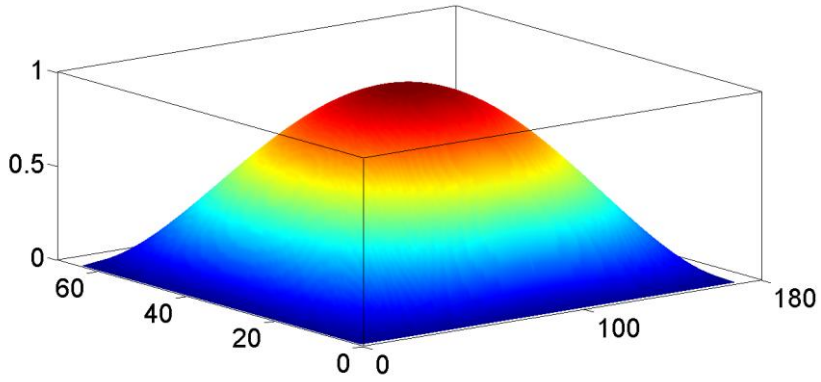

Figure 5 - Weight function for a 170 × 65 data points domain.

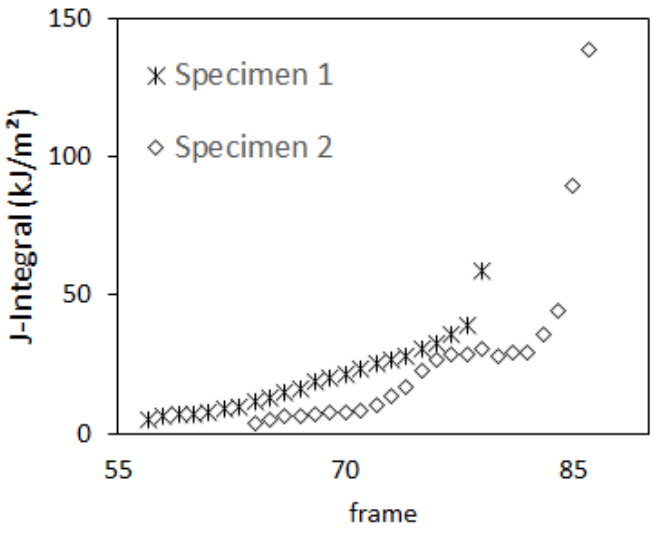

a)

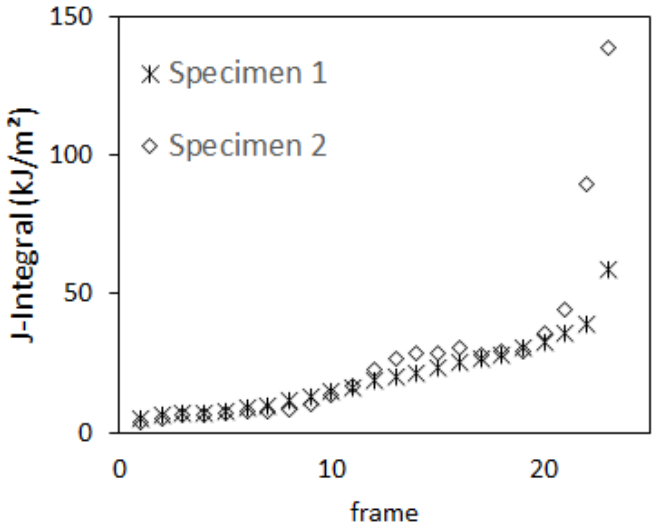

b)

Figure 6 - J-Integral scatter over time frames, (a) original input data, (b) shifted to synchronize the peak load frame.

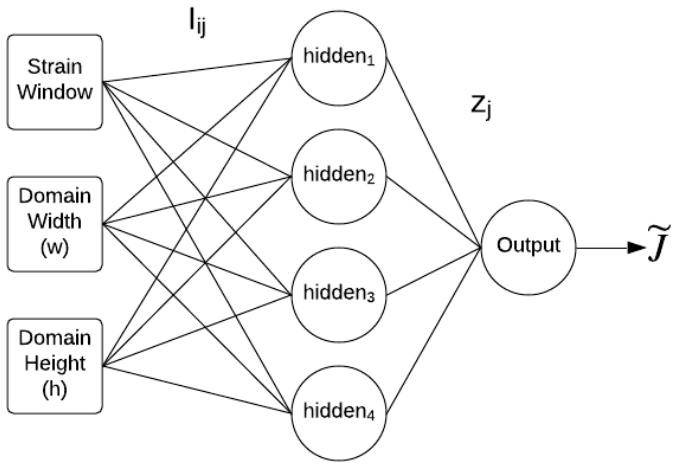

Figure 7 - Diagram of the multilayer perceptron used for $RI_{\%}$ estimates.

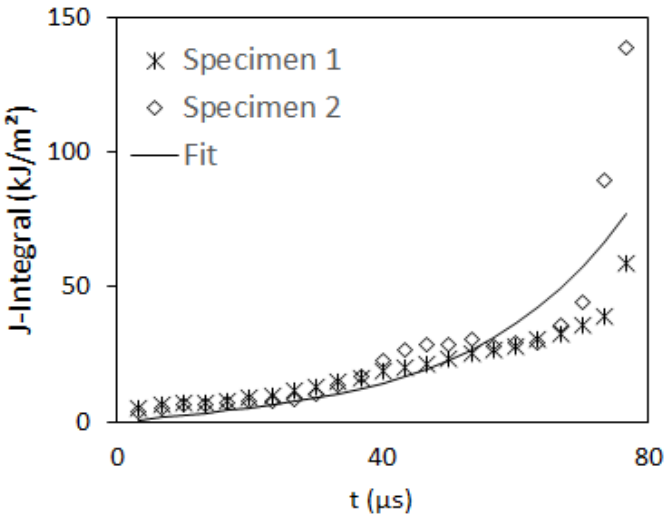

Figure 8 - J-Integral over time for type II.

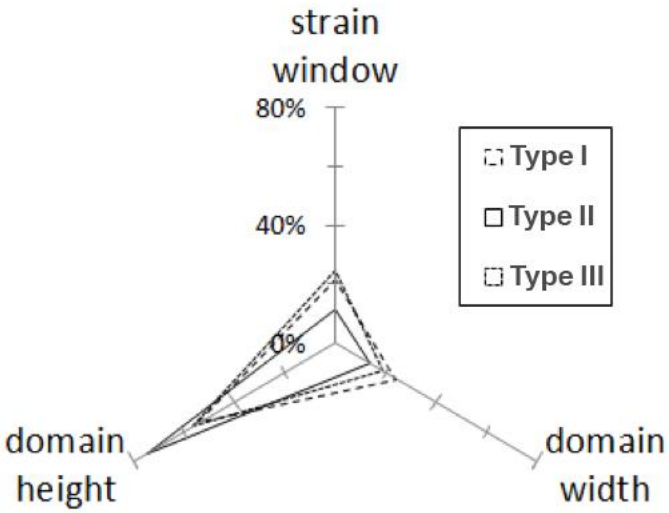

Figure 9 - Relative influence of variables on fracture toughness.

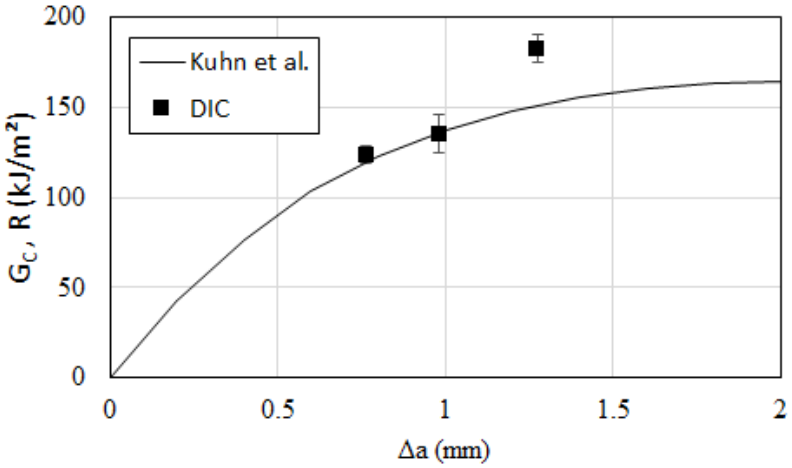

Figure 10 – G_C points obtained in the present work (DIC) and the R-Curve obtained by Kuhn *et al*. [13] for longitudinal plies.